Experimental and computational study of ethanolamine ices at astrochemical conditions

R. RAMACHANDRAN [1,2] MILAN SIL [3,4,2] PRASANTA GORAI [5,6,2] J K MEKA [1] S PAVITHRAA [7] J -I LO [8]
S -L CHOU [9] Y -J WU [9] P JANARDHAN [1] B -M CHENG [8] ANIL BHARDWAJ [1] VÍCTOR M. RIVILLA [10]
N J MASON [11] B SIVARAMAN [1] AND ANKAN DAS [2,12]

[1] *Physical Research Laboratory, India.*
[2] *Institute of Astronomy Space and Earth Sciences, P 177, CIT Road, Scheme 7m, Kolkata 700054, West Bengal, India*
[3] *Univ. Grenoble Alpes, CNRS, IPAG, 38000 Grenoble, France*
[4] *Univ Rennes, CNRS, IPR (Institut de Physique de Rennes) - UMR 6251, F-35000 Rennes, France*
[5] *Rosseland Centre for Solar Physics, University of Oslo, PO Box 1029 Blindern, 0315 Oslo, Norway*
[6] *Institute of Theoretical Astrophysics, University of Oslo, PO Box 1029 Blindern, 0315 Oslo, Norway*
[7] *Department of Applied Chemistry and Institute of Molecular Sciences, National Chiao Tung University, Hsinchu, Taiwan.*
[8] *Department of Medical Research, Hualien Tzu Chi Hospital, Buddhist Tzu Chi Medical Foundation, Hualien, Taiwan.*
[9] *National Synchrotron Radiation Research Centre, Hsinchu, Taiwan.*
[10] *Centro de Astrobiología (CSIC-INTA), Ctra. de Ajalvir Km. 4, Torrejón de Ardoz, 28850 Madrid, Spain*
[11] *Centre for Astrophysics and Planetary Science, School of Physical Sciences, University of Kent, Canterbury, CT2 7NH, UK.*
[12] *Max-Planck-Institute for extraterrestrial Physics, P.O. Box 1312 85741 Garching, Germany*

ABSTRACT

Ethanolamine ($NH_2CH_2CH_2OH$) has recently been identified in the molecular cloud G+0.693-0.027, situated in the SgrB2 complex in the Galactic center. However, its presence in other regions, and in particular in star-forming sites, is still elusive. Given its likely role as a precursor to simple amino acids, understanding its presence in the star-forming region is required. Here, we present the experimentally obtained temperature-dependent spectral features and morphological behavior of pure ethanolamine ices under astrochemical conditions in the $2-12$ μm (MIR) and $120-230$ nm (VUV) regions for the first time. These features would help in understanding its photochemical behavior. In addition, we present the first chemical models specifically dedicated to ethanolamine. These models include all the discussed chemical routes from the literature, along with the estimated binding energies and activation energies from quantum chemical calculations reported in this work. We have found that surface reactions: $CH_2OH + NH_2CH_2 \rightarrow NH_2CH_2CH_2OH$ and $NH_2 + C_2H_4OH \rightarrow NH_2CH_2CH_2OH$ in warmer regions ($60-90$ K) could play a significant role in the formation of ethanolamine. Our modeled abundance of ethanolamine complements the upper limit of ethanolamine column density estimated in earlier observations in hot core/corino regions. Furthermore, we provide a theoretical estimation of the rotational and distortional constants for various species (such as HNCCO, NH_2CHCO, and NH_2CH_2CO) related to ethanolamine that have not been studied in existing literature. This study could be valuable for identifying these species in the future.

Keywords: astrochemistry — molecular processes — ISM: abundances — evolution — ISM: molecules

1. INTRODUCTION

Corresponding author: R Ramachandran, A Das, B Sivaraman
ragav.kasak@gmail.com, ankan.das@gmail.com, bhala@prl.res.in

Nitrogen and oxygen-bearing complex organic molecules (COMs) in the interstellar medium (ISM) are of substantial significance as they are considered the precursors to biomolecules such as amino acids and proteins. Ethanolamine ($NH_2CH_2CH_2OH$), also called 2-aminoethanol, glycinol or monoethanolamine, is a probable precursor of simple amino acids like glycine

and alanine (Widicus et al. 2003; Wirström et al. 2007). Ethanolamine is also a phospholipid precursor, which could play a crucial role in the evolution of the first cellular membranes needed for the emergence of life on early Earth (Rivilla et al. 2021; Fiore et al. 2022). Though several amino acids, including glycine and alanine, have been discovered on meteorites (Glavin et al. 2010; Kvenvolden et al. 1971) and comet (Altwegg et al. 2016), they have been elusive in the ISM (Kuan et al. 2003; Jones et al. 2007; Cunningham et al. 2007; Belloche et al. 2008). Amino acids in the interstellar medium (ISM) could be formed from protonated amino alcohols and formic acid under suitable conditions (Ehrenfreund et al. 2001). However, a theoretical calculation by Redondo et al. (2015) revealed that the activation barrier of this reaction presents a significant challenge under interstellar conditions.

Rivilla et al. (2021) analyzed molecular data from high-sensitivity, unbiased spectral surveys conducted by the Yebes 40m and the IRAM 30m telescopes. They successfully detected ethanolamine for the first time in the interstellar medium. This detection was made towards the molecular cloud G+0.693–0.027, located in the SgrB2 complex in the Galactic Center. Previously, ethanolamine had been searched for in various star-forming regions, including several hot cores (Widicus et al. 2003; Wirström et al. 2007) and the prototypical hot corino IRAS 16293-2422 B (Nazari et al. 2024). Telescopes such as the Caltech Submillimeter Observatory, Owens Valley Radio Observatory, and Onsala 20m were utilized in these searches. Despite extensive efforts, ethanolamine remained undetected until it was identified by Rivilla et al. (2021). Before this identification, only upper bounds for its column density had been determined. Furthermore, Rivilla et al. (2021) formulated potential ice-phase formation pathways for ethanolamine based on the previous works of (Wakelam et al. 2015; Kameneva et al. 2017; Suzuki et al. 2018; Krasnokutski 2021; Ruaud et al. 2016). However, the formation pathways of interstellar ethanolamine are still poorly known.

Several ice processing experiments (Bernstein et al. 2002; Nuevo et al. 2008; Elsila et al. 2007; Ehrenfreund et al. 2001) designed to understand the amino acid formation from simple interstellar molecules have found several organic molecules, including ethanolamine, in the resulting residue (after hydrolysis).

Here, we conducted a comprehensive theoretical and experimental study to understand the formation of ethanolamine and its photochemical behavior. Our paper presents the first experimental results of the IR and VUV study of pure ethanolamine ices under astrophysi-

cal conditions. Furthermore, we have developed a chemical model to study the fate of ethanolamine formation in hot core/corino regions.

It is organized as follows: Section 2 discusses the implemented method for this study, Results and discussion are presented in Section 3, and the conclusions are summarized in Section 4.

2. METHODOLOGY AND COMPUTATIONAL DETAILS

UV photons (including VUV) are ubiquitous in the ISM and play a vital role in its photochemistry (Carrascosa et al. 2020) and astronomical observations. Infrared spectroscopy is a valuable tool because the vibrational and rotational spectra of molecules could provide unique fingerprints that can be used to identify and characterize them. In interpreting interstellar ice's chemical composition, infrared spectra are invaluable. For example, the data gathered by the JWST is often analyzed by considering the comprehensive resources available in the Leiden Ice Database for Astrochemistry (Rocha et al. 2022, LIDA). The VUV photoabsorption of astrochemical ices helps identify molecules by comparing data from spectra returned by spacecraft in the VUV region. For example, VUV spectroscopy of astrochemical ices facilitated the identification of hydrazine on Saturn's moon Rhea (Elowitz et al. 2021). In addition to these experimental studies, a coupled computational approach is needed to comprehend its formation and assess its abundance in interstellar circumstances. This section discusses the experimental and computational methods implemented in this work to study the fate of ethanolamine in interstellar conditions.

2.1. Experimental studies
2.1.1. VUV experiments

VUV photoabsorption experiments of ethanolamine ices were carried out with the VUV light from beamline BL-03 of the Taiwan Light Source (TLS) at the National Synchrotron Radiation Research Centre (NSRRC), Taiwan. The VUV light from the synchrotron was incident normal to the sample, and the light hence transmitted was passed through a glass window coated with sodium salicylate to convert the incident UV light to visible light and detect it using a photomultiplier tube (Hamamatsu R943-02), operating in a photon-counting mode. Detailed discussions of the experimental setup, liquid sample preparation, and spectral acquisition have been presented in earlier literature (Lu et al. 2008). The ethanolamine molecules of high purity (>99% purity, Sigma Aldrich) were deposited on the LiF substrate at 10 K. The LiF substrate is chosen because it is UV trans-

parent, especially in the regions of our interest. Upon deposition, a spectrum was recorded at 10 K. The sample was then heated to higher temperatures. After multiple experimental runs, we understand how the spectra change with temperature. Hence, we choose a convenient step size that best captures these changes. A heating rate of 5 K/min is utilized, and upon stabilization at each 20 K interval, the spectrum is captured to analyze variations in VUV spectral signatures ranging from 120 to 230 nm. For all the experiments in VUV, the thickness used was approx $\sim$ 20 ML.

2.1.2. *IR experiments*

The temperature-dependent infrared spectroscopy of the ethanolamine ice was carried out using the Simulator for Astro-molecules at Low Temperature (SALT) facility housed in the Physical Research Laboratory (PRL), Ahmedabad. The setup and other details are mentioned in Ramachandran et al. (2023).

Ethanolamine (>99% purity, Sigma Aldrich), available as a liquid, was used. The sample was processed by several freeze-pump-thaw cycles. Due to its good vapor pressure at room temperature (0.54 mbar at 25 °C), the usual deposition procedure (Ramachandran et al. 2023; Elowitz et al. 2021) was followed. In the first step of the experiment, the all-metal leak valve was opened in a controlled way to deposit the ethanolamine molecules on the ZnSe window, which was precooled to 7 K and subsequently monitored in-situ using FTIR spectroscopy in the mid-IR range $(4000 - 650$ cm$^{-1})$. The ice was warmed then to higher temperatures with a ramp rate of 5 K min^{-1}, and the spectra were recorded at regular intervals of 5–10 K until its sublimation. Similar deposition procedures were followed for the deposition at different temperatures (see Table 7). For variable thicknesses, the deposition time was varied while monitoring the absorbance of the most prominent peak of the ice in the mid-IR region. In basic infrared experiments, an ice thickness of approximately 57 ML was employed.

2.2. *Computational studies*
2.2.1. *Binding energies*

One of the main challenges in accurately modeling interstellar chemistry is the limited knowledge of the binding energy (BE) of interstellar species. The abundances of these species are influenced by their adsorption and desorption on grains. While no previous literature on BEs was available for ethanolamine and related species, we are attempting for the first time to provide estimated values of BE. *Ab initio* quantum chemical calculations are carried out using `Gaussian 09` and `Gaussian 16` program packages (Frisch et al.

Table 1. ZPE-corrected BEs considering water tetramer as a substrate using MP2/aug-cc-pVDZ level of theory.

Serial Number	Species	Ground State	ZPE-corrected Binding Energy (K)
1	HNCCO	singlet	3296
2	NH$_2$CCO	doublet	4935
3	NH$_2$CH	singlet	6119
4	CH$_2$OH	doublet	3864
5	C$_2$H$_4$OH	doublet	3656
6	NH$_2$CH$_2$	doublet	2987
7	NH$_2$CHCO	singlet	2357
8	NH$_2$CH$_2$CO	doublet	3044
9	NH$_2$CH$_2$CHO	singlet	4314
10	NH$_2$CH$_2$CH$_2$O	doublet	3195
11	NH$_2$CH$_2$CHOH	doublet	4509
12	NH$_2$CH$_2$CH$_2$OH	singlet	4744

2013, 2016) to compute BEs for ethanolamine and related species having undefined BEs and noted in Table 1 along with the ground state spin multiplicities. Among several structural isomers of ethanolamine (Novakovskaya & Rodnikova 2015), we consider the lowest-energy structure (g′Gg′) for all our calculations. Water ice is the dominant component of the interstellar grain mantle in the dense regions of ISM (Boogert et al. 2015). Though recent studies (Germain et al. 2022; Tinacci et al. 2022) suggest that a significant number ($\sim$ 100) of H$_2$O molecules in the amorphous solid water (ASW) cluster could simulate the realistic interstellar ice mantle, we assume the water c-tetramer structure to be a unit of ASW substrate (Das et al. 2018, showed it gives average percentage deviation from experiment $\sim \pm 18.8\%$) and single binding site despite having larger BE distribution (Heyl et al. 2022) due to a very high computational cost of computing BE distributions. The BE is typically considered a local property that results from the electronic interaction between the substrate (grain surface or adsorbent) and the species deposited on it (adsorbate). In the case of a bound adsorbate, the BE is a positive value. It is defined as the difference in the electronically optimized energy between the separated species and substrate and the adsorbed species on the substrate. The optimized energies of the species, water tetramer cluster, and complexes are calculated at the MP2/aug-cc-pVDZ level of theory (Dunning 1989). All the BE calculations are performed by optimizing every degree of freedom and using harmonic vibrational zero-point energy (ZPE) corrections to consider molecular vibration at low temperatures. It must be acknowledged that BE calculations are often far from simple approaches like this study and highly depend on the methodology used.

2.2.2. *Chemical reaction rates*

Table 2 and Figure 1 depicts some ice-phase reactions that have been proposed to lead to the formation of ethanolamine on the surface of dust grains (Rivilla et al. 2021; Charnley 2001; Wakelam et al. 2015; Kameneva et al. 2017; Suzuki et al. 2018; Krasnokutski 2021; Ruaud et al. 2016; Molpeceres & Rivilla 2022; Singh et al. 2013; Woon 2002). The radical-radical (RR) reactions can happen without any activation barrier, whereas the neutral-radical (NR) reactions have to overcome a finite amount of energy barrier to start. We calculate this ice-phase activation barrier with ZPE correction using the QST2 method by finding a transition state structure with the DFT-B3LYP/6-31+G(d,p) level of theory. Table 2 also shows the ice-phase reaction enthalpies (using same level of theory) to check whether the reactions are exothermic or endothermic. A continuum solvation field is considered to represent the ice features. The integral equation formalism (IEF) variant of the polarizable continuum model (PCM) as a default self-consistent reaction field (SCRF) method is employed with water as a continuous homogeneous dielectric medium representing the solvent (Cancès et al. 1997; Tomasi et al. 2005).

2.2.3. *Chemical modeling*

The CMMC (Chemical Model of Molecular Cloud) code (Das et al. 2015, 2019; Das et al. 2021; Gorai et al. 2017a,b, 2020; Sil et al. 2018, 2021; Bhat et al. 2021; Srivastav et al. 2022; Taniguchi et al. 2023) is implemented for studying the formation of ethanolamine. It is a time-dependent gas-grain code that considers gas and homogeneous reactive ice mantle, i.e., a two-phase model, based on the rate equation approach.

Here, the gas-phase pathways are mainly adopted from the UMIST Database for Astrochemistry 2022 (Millar, T. J. et al. 2024). Additionally, the destruction of gas phase ethanolamine and its related species by major ions (H_3^+, HCO^+, H^+, C^+, He^+ with a typical rate constant of $\sim 10^{-9}$ cm^3 s^{-1}) and photo reactions are considered (see Table A). Altogether, our gas phase network contains $\sim$ 8848 reactions between $\sim$ 750 species. A typical cosmic-ray ionization rate of the ISM $\sim 1.3 \times 10^{-17}$ s^{-1} is considered. A typical ratio between the desorption and diffusion energy of $\sim$ 0.5 is considered. Here, the surface chemistry network is primarily considered from Ruaud et al. (2016), and the BE of the surface species is considered from Garrod (2013); Das et al. (2018); Srivastav et al. (2022); Mondal et al. (2021); Wakelam et al. (2017); Sil et al. (2021). The BE set used in this work is available at https://www.iases.org.in/Ankan-web/AD-doc/BE-astrochem-kol-ver1.dat. Additionally, the ice phase reaction network contains other pathways used in Garrod et al. (2017); Belloche et al. (2014) regarding the H abstraction reactions. Moreover, we incorporate the ice phase reactions detailed in Table 2 and Figure 1 and the BE reported in Table 1. Altogether our present surface network contains 1485 reactions and $\sim$ 500 ice phase species. Various ice phase desorption mechanisms (thermal, cosmic ray induced, reactive, and photodesorption) have been considered for the desorption of the newly included species. The encounter desorption (Hincelin et al. 2015; Chang et al. 2021; Das et al. 2021) effect is considered to avoid overestimating the H_2 abundance on the grain surface. Recently, Oba et al. (2019) and Furuya et al. (2022) estimated the reactive desorption probability of H_2S and $PH_3 \sim 3 - 4$ %. However, due to our limited understanding of this parameter, a typical value $\sim$ 0.01 is adopted (Garrod 2013; Furuya et al. 2015; Das et al. 2021). Typically, low metal abundances are used for this type of model. Currently, we are utilizing the values used by Garrod (2013) for a similar model, which is based on the initial low metal elemental abundance set by Graedel et al. (1982), except for He, C^+, N, and O, for which values were derived from their diffuse cloud model. In this context, initial H, H_2, He, N, and O are considered neutral, while all other species are in their ionized form. The initial electron abundance is set equal to the total initial elemental abundances of positive ions.

Here, a physical condition is used, which is suitable to explain the environment corresponding to the surroundings of high-mass and low-mass protostars, i.e., hot core and hot corino, respectively. The physical condition of our model is divided into three distinct stages: collapse, warm-up, and post-warm-up. During the warm-up stage, the collapse halts, and dust and gas temperatures gradually increase. The time scale of this phase is primarily based on the approach of Viti et al. (2004), who used the observed protostellar luminosity function of Molinari et al. (2000) to derive effective temperatures throughout the accretion phase of a central protostar until it reaches Zero age main sequence. They approximated the compelling temperature profile as a power law concerning the protostar's age. They used contraction times determined by Bernasconi & Maeder (1996) to estimate a timescale of $10^4 - 10^6$ years for stars of 60 to 5 solar masses, respectively. The physical parameters adopted in our model are summarized in Table 6 and Figure 2. Similar physical parameters were adopted in some of the earlier studies (Garrod & Herbst 2006; Gar-

Table 2. The ice phase reaction pathways related to the formation of ethanolamine studied using the DFT-B3LYP/6-31+G(d,p) level of theory.

Reaction Number (Type)	Ice-phase/grain-surface reactions	Reaction enthalpy (kcal/mol)	Types of reaction	Activation barrier (K)	References and comments
R1 (RR)	$C_2 + O \rightarrow CCO$	-147.46^a	Exothermic	...	KIDA
R2 (RR)	$H + CCO \rightarrow HCCO$	-123.88^a	Exothermic	...	KIDA, Wakelam et al. (2015)
R3 (RR)	$H + HCCO \rightarrow H_2CCO$	-104.18^a	Exothermic	...	KIDA
R4	$H_2CCO + NH \rightarrow HNCCO + H_2$	-72.72^a	Exothermic		Rivilla et al. (2021)
R5 (RR)	$HCCO + N \rightarrow HNCCO$	-169.75^a	Exothermic	...	Charnley (2001)
R6 (NN)	$HNC + CO \rightarrow HNCCO$	22.60^a	Endothermic*	13289^{a*}	Kameneva et al. (2017)
R7a (NR)	$HNCCO + H \rightarrow NH_2CCO$	-71.99^a	Exothermic	3000^b	Rivilla et al. (2021)
R7b (RR)	$NH_2CCO + H \rightarrow NH_2CHCO$	-77.64^a	Exothermic	...	Rivilla et al. (2021)
R8 (RR)	$NH_2 + CH \rightarrow NH_2CH$	-127.64^a	Exothermic	...	Singh et al. (2013)
R9 (RR)	$NH_2CH + CO \rightarrow NH_2CHCO$	-26.33^a	Exothermic	...	Singh et al. (2013)
R10a (NR)	$NH_2CHCO + H \rightarrow NH_2CH_2CO$	-51.17^a	Exothermic	3000^b	Rivilla et al. (2021)
R10b (RR)	$NH_2CH_2CO + H \rightarrow NH_2CH_2CHO$	-89.46^a	Exothermic	...	Rivilla et al. (2021)
R11 (RR)	$NH_2CH + H \rightarrow NH_2CH_2$	-72.15^a	Exothermic	...	Rivilla et al. (2021)
R12 (NR)	$CH_2NH + H \rightarrow NH_2CH_2$	-40.78^a	Exothermic	2134^d	Woon (2002)
R13 (NN)	$NH_2CH_2 + CO \rightarrow NH_2CH_2CO$	-5.35^a	Exothermic	4227^c	Singh et al. (2013)
R14a (NR)	$NH_2CH_2CHO + H \rightarrow NH_2CH_2CH_2O$	-21.25^a	Exothermic	2369^a	Rivilla et al. (2021)
R14b (RR)	$NH_2CH_2CH_2O + H \rightarrow NH_2CH_2CH_2OH$	-102.00^a	Exothermic	...	Rivilla et al. (2021)
R15a (NR)	$NH_2CH_2CHO + H \rightarrow NH_2CH_2CHOH$	-30.85^a	Exothermic	3236^a	Rivilla et al. (2021)
R15b (RR)	$NH_2CH_2CHOH + H \rightarrow NH_2CH_2CH_2OH$	-92.40^a	Exothermic	...	Rivilla et al. (2021)
R16 (RR)	$NH_2CH_2 + CH_2OH \rightarrow NH_2CH_2CH_2OH$	-72.00^a	Exothermic	...	Rivilla et al. (2021)
R17 (NR)	$C_2H_4 + OH \rightarrow C_2H_4OH$	-27.5^e	Exothermic	710^e	Molpeceres & Rivilla (2022)
R18 (RR)	$C_2H_4OH + NH_2 \rightarrow NH_2CH_2CH_2OH$	-79.81	Exothermic	...	Molpeceres & Rivilla (2022)

[a] Calculated in this work.

* Due to the high endothermicity of this reaction, it is not considered in our network.

[b] Assumed in this work.

[c] Singh et al. (2013).

[d] Woon (2002).

[e] Molpeceres & Rivilla (2022).

Table 3. Dipole moments using DFT-B3LYP/6-311++G(d,p) level of theory.

Species	Dipole moments (in D)			
	μ_a	μ_b	μ_c	μ_{tot}
HNCCO	1.15	0.82	0.00	1.42
NH_2CHCO	-2.24	1.41	0.00	2.65
NH_2CH_2CO	-2.57	1.45	1.24	3.20
$NH_2CH_2CH_2OH$	$-3.00 \ (2.65)^a$	$1.14 \ (0.89)^a$	$0.55 \ (0.42)^a$	$3.25 \ (2.82)^a$

Note: [a] Absolute values of the total dipole moment and its components predicted by Penn & Curl (1971).
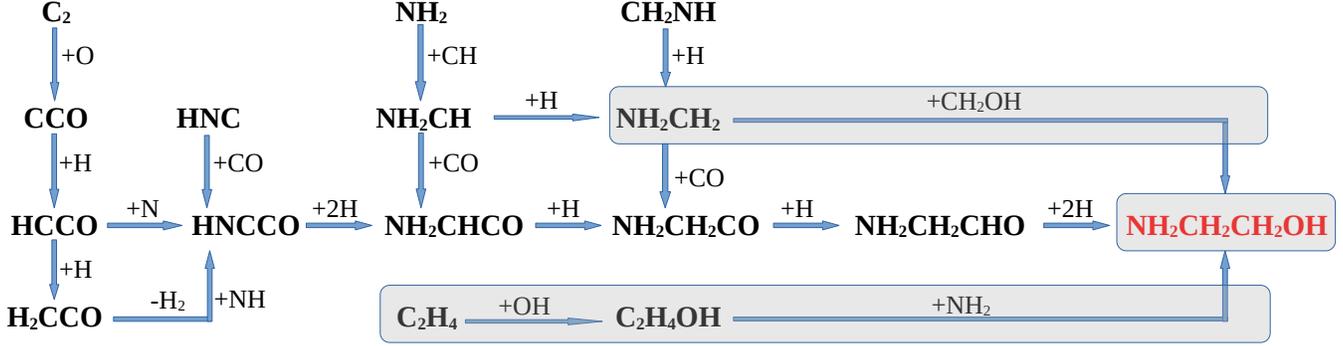
Figure 1. Summary of proposed chemical routes leading to the formation of ethanolamine on dust grain surfaces. The grey-shaded area corresponds to the most viable ice-phase routes for the formation of ethanolamine according to the chemical model presented here. Only the formation of ice phase ethanolamine is emphasized here. We note that the destruction by major ions and UV photons (including cosmic-ray-induced ones) is not shown in this diagram, but they are considered in the chemical models.

Table 4. Ground vibrational and equilibrium rotational constants and asymmetrically reduced quartic centrifugal distortion constants of HNCCO, NH_2CHCO, NH_2CH_2CO, and $NH_2CH_2CH_2OH$ with the DFT-B3LYP/6-311++G(d,p) level of theory.

Sl. No.	Species	Rotational constants	Calculated values (in MHz)	Distortion constants	Calculated values (in MHz)
1.	HNCCO (Singlet)	A_0	268915.214	D_N	-0.00039892657
		B_0	4499.747	D_K	-1034.5240
		C_0	4367.401	D_{NK}	-2.4075581
		A_e	219743.385	d_N	0.00011340140
		B_e	4476.900	d_K	-0.58283144
		C_e	4387.512		
2.	NH_2CHCO (Singlet)	A_0	43671.751	D_N	-0.0022392657
		B_0	4608.267	D_K	-0.71283617
		C_0	4283.586	D_{NK}	-0.16315747
		A_e	44190.690	d_N	-0.00078731244
		B_e	4634.836	d_K	-0.015381555
		C_e	4292.983		
3.	NH_2CH_2CO (Doublet)	A_0	42231.836	D_N	-0.001274949
		B_0	4232.048	D_K	-0.73808078
		C_0	3984.143	D_{NK}	-0.0060688055
		A_e	42425.597	d_N	-0.000071558688
		B_e	4264.891	d_K	-0.0090472182
		C_e	4019.650		
4.	$NH_2CH_2CH_2OH$ (Singlet)	A_0	14401.029	D_N	-0.0061629178
		B_0	5429.504	D_K	-0.048060075
		C_0	4479.870	D_{NK}	0.020970813
		A_e	14460.409 (14508.73 ± 0.1^a)	d_N	-0.0018253369
		B_e	5538.498 (5546.46 ± 0.04^a)	d_K	-0.011234133
		C_e	4552.708 (4570.46 ± 0.03^a)		

Note: [a] Penn & Curl (1971)

Table 5. Comparing IR peak positions in the ice phase (from this work) with that of the previously available in (Jackson et al. 2009, pure liquid phase experiment and theoretical gas phase) and (Krueger & Mettee 1965, in C_2Cl_4 solution).

Peak position(cm^{-1})				
This work		Previous works		
Experiment		Pure Liquid phase	in C_2Cl_4 solution	Theoretical gas phase
7 K	180 K	Jackson et al. (2009)	Krueger & Mettee (1965)	Jackson et al. (2009)
			3640	3644
			3624	3612
			3526	3508
			3411	
3352	3314	3355	3340	
3287	3268	3293		
3201	3182			
	3136			3036
	3073			2995
2936	2911	2927		2956
2861	2874	2864		2948
2786	2768			
2726	2735			
2658	2670			
	2642			
	2567			
	2513			
1684	1674			1672
1606	1615	1601		
1460	1489	1461		1465
	1452			
1395	1385			1405
1360	1362	1355		
	1348			
	1310			
	1294			
1254	1257			
1174	1160	1172		1198
1083	1119	1081		
	1101			1101
	1066			1060
1035	1030	1033		
	986			999
970	962			
872	874			
	839			
	774			
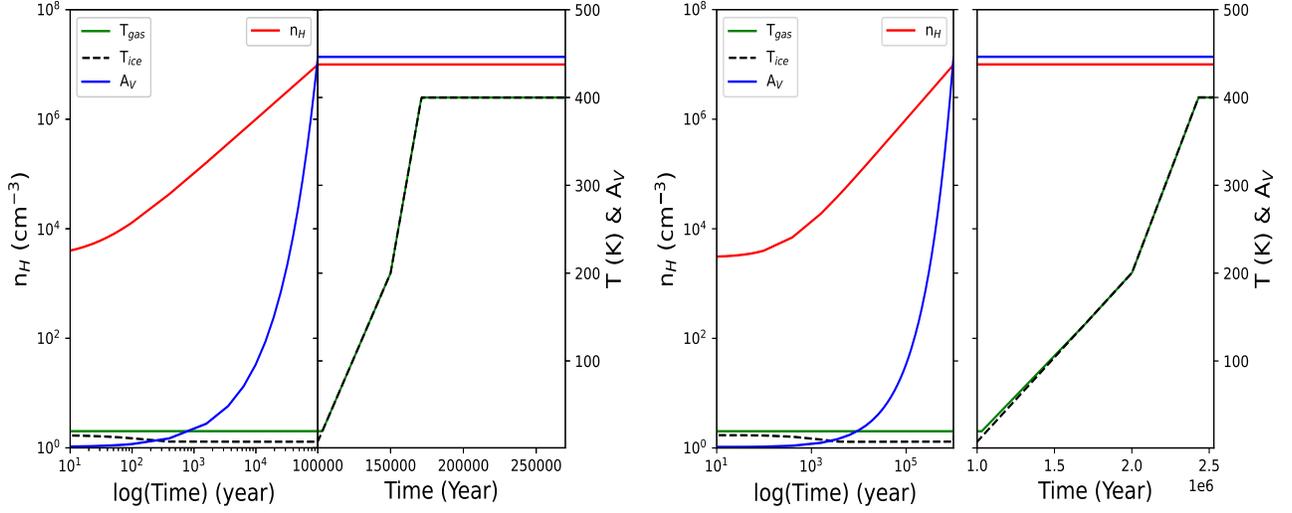
Figure 2. The adopted physical conditions for a hot core (left panel) and hot corino (right panel) region.

Table 6. Adopted physical parameters considered in our model.

	hot core	hot corino
	Collapse phase	
$t_{coll}(yr)$	10^5	10^6
$n_{H min}(cm^{-3})$	3.0×10^3	3.0×10^3
$n_{H max}(cm^{-3})$	10^7	10^7
Tgas(K)	20	20
A_V	$A_{V0}(n_H/n_{H min})^{2/3}(A_{V0}=2)$	$A_{V0}(n_H/n_{H min})^{2/3}(A_{V0}=2)$
Tice(K)	Zucconi et al. (2001); Garrod (2008)	Zucconi et al. (2001); Garrod (2008)
	1st warm-up phase	
$t_{warm1}(yr)$	5.0×10^4	10^6
$n_H(cm^{-3})$	10^7	10^7
$Tgas_{min}(K)$	20	20
$Tgas_{max}/Tice_{max}$ [b] (K)	200	200
$Tice_{min}(K)$	$Tice_{min}$ [a]	$Tice_{min}$ [a]
A_V	$A_{V max}$ [a]	$A_{V max}$ [a]
	2nd warm-up phase	
$t_{warm2}(yr)$	2.1×10^4	4.3×10^5
$n_H(cm^{-3})$	10^7	10^7
$Tgas_{min}/Tice_{min}(K)$	200	200
$Tgas_{max}/Tice_{max}$ [b] (K)	400	400
A_V	$A_{V max}$ [a]	$A_{V max}$ [a]
	post-warm-up phase	
$t_{pw}(yr)$	10^5	10^5
$n_H(cm^{-3})$	10^7	10^7
Tgas(K)	400	400
Tice(K)	400	400
A_V	$A_{V max}$ [a]	$A_{V max}$ [a]
Total simulation time	2.712×10^5	2.53×10^6

Notes: [a] Obtained at the end of the collapsing phase.
[b] A linear relationship between temperature increase and time is being considered.

rod 2013; Garrod et al. 2017; Gorai et al. 2020; Mondal et al. 2021; Srivastav et al. 2022; Taniguchi et al. 2023).

2.2.4. *Microwave rotational spectroscopy*

Several of the proposed precursors of ethanolamine have not had their rotational spectroscopy measured (see Figure 1). Therefore, we are presenting the theoretical calculations of its dipole moments and rotational constants to aid future laboratory experiments. Rotational spectroscopy is the primary tool to detect species in the ISM. Almost 80% of the observed species having permanent electric dipole moments are detected from their rotational transitions (McGuire 2022). The intensity of any rotational transition is directly and inversely proportional to the square of the dipole moment and the rotational partition function, respectively. Dipole moment components along the inertial axis and total dipole moments of ethanolamine and related molecules (HNCCO, NH_2CHCO, and NH_2CH_2CO, for which no data were available in the literature) calculated using DFT-B3LYP/6-311++G(d,p) level of theory are summarized in Table 3. In accordance with the experimental work by Penn & Curl (1971), a very strong a-type dipole moment for ethanolamine is obtained, while the b-type and c-type lines are generally much weaker, indicating that ethanolamine has a predominant dipole moment along one principal axis, which has implications for its spectroscopic properties and structural characteristics. However, we note some deviations in the dipole moments compared to the values reported by Penn & Curl (1971). This suggests that employing a high-cost functional and basis set combination could help reduce these deviations, which is beyond the scope of this work. The values obtained by Penn & Curl (1971) for ethanolamine are based on experiments and could be considered more accurate. Our calculated dipole moments for HNCCO, NH_2CHCO, and NH_2CH_2CO are relatively high (see Table 3), which would help to detect the molecules once the rotational spectroscopy is measured in the future.

The ground vibrational (A_0, B_0, C_0) and equilibrium (A_e, B_e, C_e) values of rotational constants and asymmetrically reduced quartic centrifugal distortion constants (D_N, D_K, D_{NK}, d_N, d_K) are also calculated for these species using the same level of theory and noted in Table 4. The percentage deviations of the rotational constants A, B, and C calculated in our work compared to those in Penn & Curl (1971) are underpredicted by 0.33%, 0.14%, and 0.39%, respectively. These small percentage deviations indicate a high degree of consistency between the two sets of results. Based on this, we provide the rotational spectroscopic constants for its re-
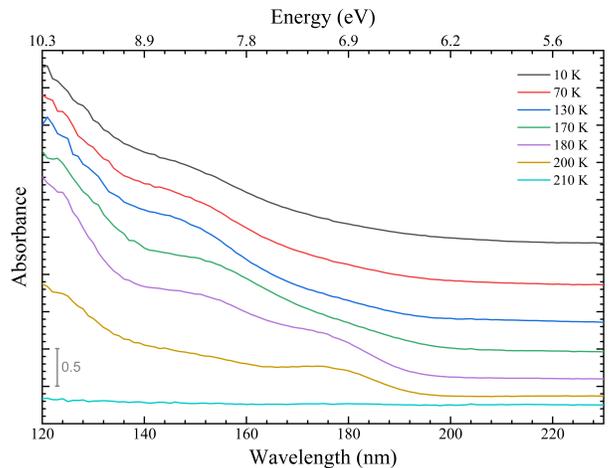
Figure 3. Experimental VUV spectra of ethanolamine ices (stacked) in the 120 - 240 nm range for a selected set of temperatures

.

lated species, HNCCO, NH_2CHCO, and NH_2CH_2CO, for which no values were available in the literature.

3. RESULTS AND DISCUSSION

3.1. *Experimental results*

3.1.1. *VUV spectra of pure ethanolamine ice*

Figure 3 presents the stacked temperature-dependent VUV spectra of ethanolamine ice deposited at 10 K in the $120 - 230$ nm range and subsequently warmed to higher temperatures.

At 10 K, we observe that the spectrum has a weak band/bump between 141 and 157 nm and beyond 210 nm, there is no absorption. When warmed to higher temperatures, the spectra show no noticeable changes in the spectra until 100 K. On warming the ice to 130 K, we could observe that the band centered around 142 nm became more prominent while the peak positions remained unchanged. On further warming to 180 K, the spectrum peaked at 172 nm. At 180 K, the infrared red spectrum reveals an onset phase change. The two distinct bands could be due to the dimer, monomer forms of the ethanolamine, as mentioned earlier in the case of formamide ice (Sivaraman et al. 2012). Upon warming to 200 K, spectra recorded clearly show a completely crystalline phase, and beyond 210 K, the ice sublimes.

3.1.2. *IR spectra of pure ethanolamine ice*

Figure 4 depicts the temperature-dependent stacked IR spectra of ethanolamine ice deposited at 7 K between 3600 cm^{-1} and 750 cm^{-1}. When deposited at 7 K, several peaks are noticed in two regions, one between 3600 cm^{-1} and 2500 cm^{-1} and the other between
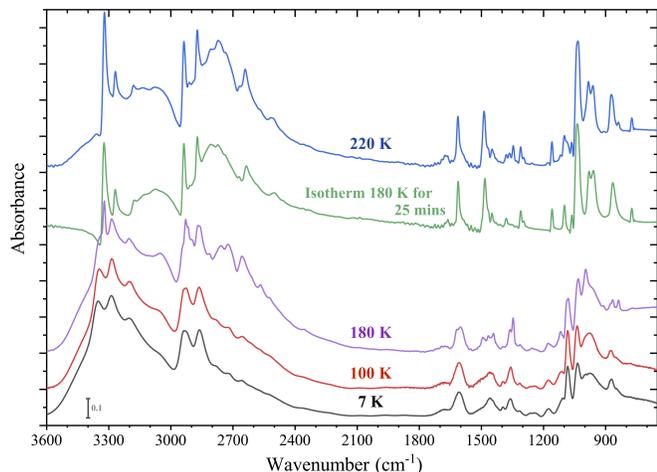
Figure 4. Temperature dependent experimental IR spectra of ethanolamine ices.

1700 cm^{-1} and 800 cm^{-1}. The 1st column of Table 5 presents the positions of all these observed peaks. In the absence of any previous ice-phase spectra, comparing this with the previous liquid phase and gas-phase results, the peak positions of pure ethanolamine at 10 K are in good agreement with that of the pure liquid phase of Jackson et al. (2009), and also with their theoretical gas-phase values. We see no significant difference up to 180 K after heating to higher temperatures. At 180 K, we see clear evidence of compaction of the ethanolamine ice, and when kept at 180 K for about 25 minutes, the phase change (amorphous/metastable to crystalline) is noticed. When this spectrum (isotherm at 180 K for 25 min spectrum of Fig 4) is compared with other spectra at lower temperatures, many additional peaks and sharper peaks are noticed. These are a result of the re-orientation of ethanolamine molecules in the ice. The ice wholly sublimated at 230 K.

Another exciting aspect of ethanolamine ice is its dependence on the thickness of the ice. The upper panel of Figure 5 illustrates the deposition of ethanolamine ice at 7 K, while the lower panel displays it for 190 K. The observation indicates that at the lower deposition temperature, several additional peaks (indicated by arrows in the upper panel of Figure 5) are present for the thick ice, which were absent in the thin ice.

A more detailed and quantitive study is needed to understand the origin and assignments for these peaks, nonetheless, it is a noteworthy observation. At 190 K (lower panel of Figure 5), evidence of phase change is noticed in almost all the new peaks in the thick ice at 7 K. Since some regions are already saturated, all the peaks are not seen. To further understand the behav-

ior of ethanolamine ices, we performed several cycles of experiments by changing different variables like deposition temperature, deposition time, isotherm temperature, and isotherm time, a few results of which are shown in Table 7. From a series of experiments summarised in Table 7, we can infer that irrespective of the deposition time or rate of warming, the phase change temperature remains the same (190 K) when the ethanolamine ice is deposited at 7 K. The same ice deposited at 7 K, when kept at isotherm at 180 K for $\sim$ 4 hrs, it changes from amorphous to crystalline at 180 K itself. But when kept at isotherm at 170 K, the phase change does not occur even after 7 hrs. This shows that the phase change process initiates around 175 K, but it is a slow process and hence requires more energy, which it could either get from higher thermal energy (higher temperature) or cumulative energy due to isotherm at any temperature above 175 K.

3.2. *Computational results*

3.2.1. *Chemical modeling of hot core*

Our quantum chemical calculations have revealed that all the reactions mentioned in Table 2 are exothermic. Among these reactions, the neutral-radical reactions possess activation barriers. These activation barriers have been estimated and directly incorporated into our model. In addition, some other reactions are presented based on our study. For the ice-phase synthesis of H_2CCO, the barrierless reactions R1-R3 are considered from KIDA. Charnley (2001) proposed the formation of HNCCO by the reaction between HCCO and N (reaction R5). This radical-radical (RR) reaction can happen at each encounter without any activation barrier. It is noticed that this reaction is exothermic, having reaction enthalpy -169.75 kcal/mol. Rivilla et al. (2021) proposed reaction R4 for the formation of HNCCO. Kameneva et al. (2017) suggested the neutral-neutral (NN) reaction between HNC and CO (reaction R6). However, our calculation exhibits it as an endothermic reaction (22.60 kcal/mol). Also, with the transition state calculation, it is noticed that it possesses a very high activation barrier ($\sim$ 13289 K). In our reaction network, reaction R6 is not considered for forming HNCCO. Two successive hydrogenations of HNCCO are required to produce NH_2CHCO. The first step (R7a) is the neutral-radical (NR) reaction, and the second step (R7b) is the RR reaction. Both reactions are found to be exothermic. Since the second reaction is RR, it will process as barrierless. But the first reaction should contain some activation barrier. However, an actual transition state of the reaction R7a is not obtained. Therefore, a conservative value of 3000 K is considered an educated

Table 7. Log of IR experiments carried out at different temperatures and thicknesses and different isotherm temperatures and durations.

Dep. temp. (K)	Dep. time (sec)	Phase change (K)	Ramp rate (K/min)	Sublimation (K)	Isothermal temp. and duration	Remarks
7	220	190	10	$235 - 240$	—	—
7	903	190	5	230	—	—
7	425	190	5	230	—	—
7	435	180	5	230	180 K, 4 hrs	Crystalline within 4 hrs of isothermal at 180 K
170	2400	190	5	230	170 K, 7 hrs	Compaction after 2 hrs, No crystallization even after 7 hrs.
175	1500	175	5	220	175 K, 90 min	The ice turned crystalline
180	1200	180	5	230	—	Fully crystalline ice
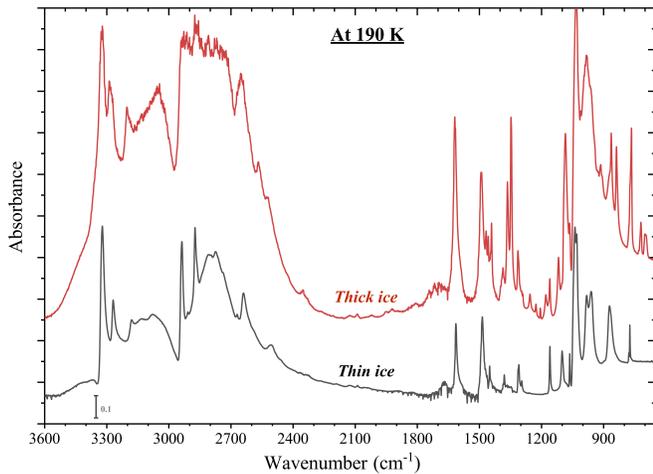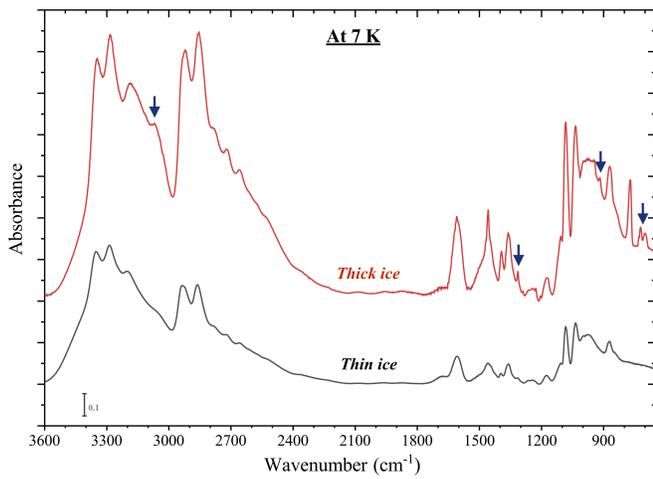
Figure 5. Comparison of Experimental IR spectra of Thin and Thick ethanolamine ices at 7 K (upper panel) and after warming to 190 K (lower panel). The additional peaks in thick ice appearing at 7 K have been marked with blue arrows.
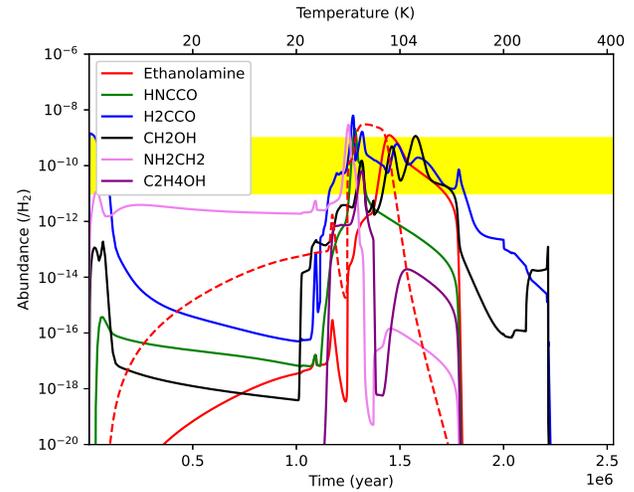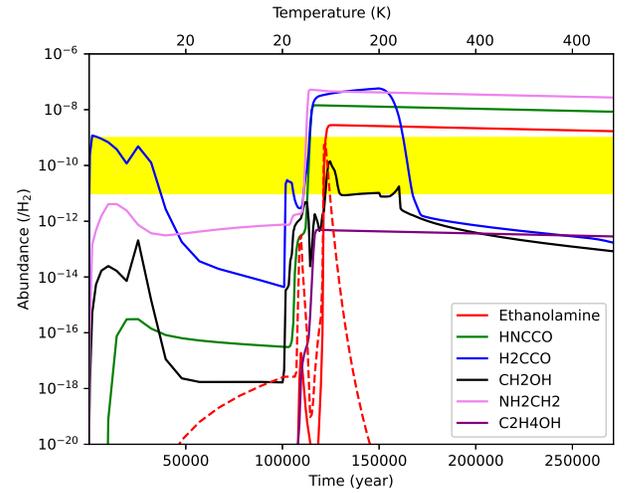
Figure 6. Time evolution of the ethanolamine abundances and some related species (HNCCO, H_2CCO, CH_2OH, NH_2CH_2, C_2H_4OH) for hot core (upper panel) and hot corino region (lower panel). The dashed line represents the ice phase ethanolamine abundance .

estimation for the activation barrier of this reaction. The effect of this barrier is also discussed afterward.

There are other alternative pathways to form NH_2CHCO by the reactions R8 and R9 (Singh et al. 2013). Both these RR reactions are barrierless and exothermic. Therefore, these pathways are also considered in our network. NH_2CHCO is further processed through two successive hydrogenations (R10a and R10b) to form NH_2CH_2CHO. The first reaction (R10a) should contain the activation barrier. However, we could not get an actual transition state and consider the 3000 K barrier for R10a. At the same time, the second RR reaction, R10b, is barrierless and can be processed without an activation barrier.

The reactions R11-R13 provide another alternative formation pathway for NH_2CH_2CO, where R11 is RR barrierless exothermic reaction and R12 is NR exothermic possessing a barrier of 2134 K (Woon 2002). Following Singh et al. (2013), we consider the ice-phase NN reaction R13 with an activation barrier 4227 K. Hydrogenation of NH_2CH_2CHO can happen in two possible locations (C or O atom positions) and form $NH_2CH_2CH_2O$ (R14a) or NH_2CH_2CHOH (R15a). Quantum chemical calculations yield activation barriers of 2369 K and 3236 K for R14a and R15a, respectively. $NH_2CH_2CH_2O$ and NH_2CH_2CHOH further react with another hydrogen atom and form the target product ethanolamine (reactions R14b and R15b). Both of these RR reactions are found to be exothermic. The exothermic reaction R16 between two radicals NH_2CH_2 and CH_2OH to form ethanolamine as proposed by Rivilla et al. (2021) are included in our network. Recently, Molpeceres & Rivilla (2022) proposed two subsequent surface reactions in forming ethanolamine by $C_2H_4 + OH \rightarrow C_2H_4OH$ (R17, NR reaction) and $C_2H_4OH + NH_2 \rightarrow NH_2CH_2CH_2OH$ (R18, RR reaction). Furthermore, we consider an additional ice phase barrier less reaction between $NH_2CH_2CH_2OH$ and HCOOH for the formation of $\beta-$alanine.

Figure 6 shows the abundances of ethanolamine along with some of its related species (HNCCO, H_2CCO, CH_2OH, NH_2CH_2, and C_2H_4OH) obtained from our model. The lower X-axis in Figure 6 shows the time, the upper X-axis shows gas temperature, and the Y-axis represents the abundance with respect to H_2. The upper and lower panels represent the time evolution of abundances for hot core and hot corino regions, respectively. Dashed lines show the abundance of ethanolamine in the absence of the reaction R16. Since the hydrogenation reaction by physisorption is not generally efficient beyond 20 K, we find a significant contribution of ethanolamine by the surface reaction between CH_2OH and NH_2CH_2

(reaction R16). In the absence of the reaction number R16, ethanolamine formation is dominated by another surface reaction between C_2H_4OH and NH_2 (reaction number R18).

In the case of a hot core, we consider a fast collapsing and a fast warm-up time scale. The upper panel of Figure 6 shows that a peak abundance of $\sim 2.8 \times 10^{-9}$ could be achieved around 100 K for a hot core region. We notice that most of the ice phase formation of ethanolamine happens here between $60 - 90$ K (red dashed line in Figure 6 depicts ice phase ethanolamine). Due to a shorter warm-up time scale, its destruction would not have taken place for a long period; as a result, we can see a healthy abundance of ethanolamine at the end of the simulation. On the contrary, we consider a slow collapsing and warm-up time scale for the hot corino (lower panel of Figure 6). It shows a peak abundance of 1.2×10^{-9} around 90 K and then dramatically declines. It is worth noting that gas-phase ethanolamine production is predominantly influenced by ice-phase reaction R16 and its subsequent desorption.

We initially set the density at 3×10^3 cm^{-3} and utilized low metal initial abundances, typically considered the standard for hot core/corino models. To assess the impact of the initial density on our calculation, we also experimented with an initial density of 10^4 cm^{-3}. However, this alternative did not result in any noticeable deviation. This is because ethanolamine production is predominantly influenced during the warmup phase when the density is 10^7 cm^{-3}.

3.3. *Astronomical implications*

Ethanolamine has been only detected so far towards a molecular cloud in the Galactic Center, G+0.693-0.027 (Rivilla et al. 2021), with an abundance compared to H_2 of $\sim 10^{-10}$. It has also been searched for toward star-forming regions, including several hot cores (Widicus et al. 2003; Wirström et al. 2007), and the prototypical hot corino IRAS 16293-2422 B (Nazari et al. 2024), but the molecule was not detected, allowing only to compute upper limits for its abundance. Widicus et al. (2003) used the 10m telescope of the Caltech Submillimeter Observatory (CSO), and interferometric observations of the Owens Valley Radio Observatory (OVRO), while Wirström et al. (2007) used the Onsala 20m telescope. To convert the column density upper limits reported in these works into abundances we have used the values observed towards Orion KL. For the single-dish observations, we have corrected the beam dilution since it is expected that the spatial extent of the ethanolamine is compact as other complex molecules. For the size of the emission and the asso-

ciated value of $N(H_2)$ in the same volume, we have used the values derived for the Orion KL hot core by Feng et al. (2015) and Crockett et al. (2014), which are, respectively, $10''\times 10''$ and 3.1×10^{23} cm^{-2}, and $3.49''\times 2.57''$ and 2.3×10^{24} cm^{-2}. We obtain that the CSO observations provide an upper limit for the abundance of ethanolamine of $< (1.3 - 1.8) \times 10^{-9}$, while the Onsala observations give slightly higher values of $< (4.1 - 5.8) \times 10^{-9}$. However, we note that these numbers should be taken with caution, given the uncertainties of the size and $N(H_2)$ assumptions. The OVRO observations of Widicus et al. (2003) were centered towards the Orion Compact Ridge, so in this case, we have used the size and $N(H_2)$ derived by Feng et al. (2015) in this source, which is $3.49''\times 2.57''$ and 1.28×10^{24} cm^{-2}, respectively. The beam of the observations was $6.8''\times 4.8''$. After applying the beam dilution, we obtain an upper limit of ethanolamine abundance of $< 1.8 \times 10^{-10}$, which is at least one order of magnitude lower than that derived from the single-dish observations and very similar to the value calculated by Rivilla et al. (2021) towards G+0.693. Therefore, deep searches of ethanolamine towards hot cores are needed to establish if it is equally abundant than in G+0.693, or alternatively, this species has lower abundances in these environments. Our hot core model predicts a peak abundance of $\sim 2.8 \times 10^{-9}$. Moreover, Nazari et al. (2024) estimated an upper limit of ethanolamine column density $< 6 \times 10^{14}$ cm^{-2} towards IRAS 16293-2422 B using ALMA. Considering a H_2 column density of $\sim 10^{25}$ cm^{-2} (Jørgensen et al. 2016), it yields an upper limit of abundance $< 6 \times 10^{-11}$. This indicates that the species is less abundant in this hot corino than in G+0.693. However, our hot corino model predicts a peak abundance of $\sim 1.2 \times 10^{-9}$. For the sake of simplicity, ethanolamine abundances in the surroundings of the hot core and hot corino region would vary between $10^{-11} - 10^{-9}$. This limit is highlighted with the yellow horizontal bar in Figure 6. Since the nondetection of ethanolamine towards hot cores/corinos was possibly due to a lack of sensitivity, more high sensitivity and high-resolution spectral data could lead to its future identification. Furthermore, the high line density in these hot environments might be contributing to preventing the detection of ethanolamine, since its weak expected lines can be severely blended by stronger lines from more abundant species. To alleviate this, searches at lower frequencies, for instance in the new ALMA band 3, might help.

Apart from star-forming regions, ethanolamine has been detected in the Almahata Sitta meteorite (Glavin et al. 2010). This suggests the presence of ethanolamine in solar system objects. The IR spectra presented for ethanolamine ices would help augment the JWST data toward understanding the origin of a phospholipid precursor in solar system objects.

4. CONCLUSION

Theoretical and experimental work has been conducted to comprehend the formation of ethanolamine and its photochemistry under interstellar conditions. The major conclusions of this work are highlighted below:

- In this study, we present the first temperature-dependent VUV and mid-IR spectra of pure ethanolamine ices under astrochemical conditions. Our results show a close correspondence between the VUV and IR spectra in relation to phase change (occurring around 180 K) and sublimation (occurring around 230 K). We have observed that the phase change is greatly influenced by the deposition temperature and the isothermal condition. The VUV and IR spectral features outlined in this paper can be valuable for its future identification of ethanolamine in the interstellar ices and other cold regions of planetary and cometary bodies.

- Quantum chemical calculations are carried out to study the feasibility of ice-phase reactions involving the formation of ethanolamine. Some of these reactions contain activation barriers, which are estimated by our quantum chemical calculations. The obtained values are directly used in the model.

- Ethanolamine formation in high-mass and low-mass star-forming regions is explored by chemical models. It depicts that the formation of ethanolamine by RR surface reactions in the warmer regions $(60-90$ K) is favorable. Our modeled abundances are consistent with the estimated upper limit of ethanolamine abundance in the hot core/corino surroundings.

- To assist the interstellar search of several proposed precursors of ethanolamine (HNCCO, NH_2CHCHO, and NH_2CH_2CO), and to allow a proper derivation of the column densities from observations, we have performed theoretical calculations to derive their dipole moments, and their rotational constants. Upon reassessing the calculated rotational constants for ethanolamine and aligning them with prior data (Penn & Curl 1971), we have extended our analysis to encompass the rotational and distortional constants for these species, which were absent in the literature.

REFERENCES

Altwegg, K., Balsiger, H., Bar-Nun, A., et al. 2016, Science Advances, 2, e1600285, doi: 10.1126/sciadv.1600285

Belloche, A., Garrod, R. T., Müller, H. S. P., & Menten, K. M. 2014, Science, 345, 1584, doi: 10.1126/science.1256678

Belloche, A., Menten, K. M., Comito, C., et al. 2008, A&A, 482, 179, doi: 10.1051/0004-6361:20079203

Bernasconi, P. A., & Maeder, A. 1996, A&A, 307, 829

Bernstein, M. P., Dworkin, J. P., Sandford, S. A., Cooper, G. W., & Allamandola, L. J. 2002, Nature, 416, 401

Bhat, B., Gorai, P., Mondal, S. K., Chakrabarti, S. K., & Das, A. 2021, Advances in Space Research, doi: https://doi.org/10.1016/j.asr.2021.07.011

Boogert, A. C. A., Gerakines, P. A., & Whittet, D. C. B. 2015, ARA&A, 53, 541, doi: 10.1146/annurev-astro-082214-122348

Cancès, E., Mennucci, B., & Tomasi, J. 1997, Journal of Chemical Physics, 107, 3032, doi: 10.1063/1.474659

Carrascosa, H., Cruz-Díaz, G. A., Muñoz Caro, G. M., Dartois, E., & Chen, Y.-J. 2020, Monthly Notices of the Royal Astronomical Society, 493, 821, doi: 10.1093/mnras/staa334

Chang, Q., Zheng, X.-L., Zhang, X., et al. 2021, Research in Astronomy and Astrophysics, 21, 039, doi: 10.1088/1674-4527/21/2/39

Charnley, S. 2001, in The Bridge Between the Big Bang and Biology: Stars, Planetary Systems, Atmospheres, Volcanoes: Their Link to Life, ed. F. Giovannelli, 139

Crockett, N. R., Bergin, E. A., Neill, J. L., et al. 2014, The Astrophysical Journal, 787, 112, doi: 10.1088/0004-637X/787/2/112

Cunningham, M. R., Jones, P. A., Godfrey, P. D., et al. 2007, MNRAS, 376, 1201, doi: 10.1111/j.1365-2966.2007.11504.x

Das, A., Gorai, P., & Chakrabarti, S. K. 2019, A&A, 628, A73, doi: 10.1051/0004-6361/201834923

Das, A., Majumdar, L., Sahu, D., et al. 2015, apj, 808, 21, doi: 10.1088/0004-637X/808/1/21

Das, A., Sil, M., Ghosh, R., et al. 2021, Frontiers in Astronomy and Space Sciences, 8, 78, doi: 10.3389/fspas.2021.671622

Das, A., Sil, M., Gorai, P., Chakrabarti, S. i. K., & Loison, J. C. 2018, ApJS, 237, 9, doi: 10.3847/1538-4365/aac886

Dunning, Thom H., J. 1989, JChPh, 90, 1007, doi: 10.1063/1.456153

Ehrenfreund, P., Bernstein, M. P., Dworkin, J. P., Sandford, S. A., & Allamandola, L. J. 2001, The Astrophysical Journal, 550, L95

Elowitz, M., Sivaraman, B., Hendrix, A., et al. 2021, Science Advances, 7, eaba5749

Elsila, J. E., Dworkin, J. P., Bernstein, M. P., Martin, M. P., & Sandford, S. A. 2007, The Astrophysical Journal, 660, 911

Feng, S., Beuther, H., Henning, T., et al. 2015, A&A, 581, A71, doi: 10.1051/0004-6361/201322725

Fiore, M., Chieffo, C., Lopez, A., et al. 2022, Astrobiology, 22, 598, doi: 10.1089/ast.2021.0059

Frisch, M. J., Trucks, G. W., Schlegel, H. B., et al. 2013, Gaussian 09 Revision D.01

—. 2016, Gaussian 16 Revision B.01

Furuya, K., Aikawa, Y., Hincelin, U., et al. 2015, A&A, 584, A124, doi: 10.1051/0004-6361/201527050

Furuya, K., Oba, Y., & Shimonishi, T. 2022, ApJ, 926, 171, doi: 10.3847/1538-4357/ac4260

Garrod, R. T. 2008, A&A, 491, 239, doi: 10.1051/0004-6361:200810518

—. 2013, ApJ, 765, 60, doi: 10.1088/0004-637X/765/1/60

Garrod, R. T., Belloche, A., Müller, H. S. P., & Menten, K. M. 2017, A&A, 601, A48, doi: 10.1051/0004-6361/201630254

Garrod, R. T., & Herbst, E. 2006, A&A, 457, 927, doi: 10.1051/0004-6361:20065560

Germain, A., Tinacci, L., Pantaleone, S., Ceccarelli, C., & Ugliengo, P. 2022, ACS Earth and Space Chemistry, 6, 1286, doi: 10.1021/acsearthspacechem.2c00004

Glavin, D. P., Aubrey, A. D., Callahan, M. P., et al. 2010, M&PS, 45, 1695, doi: 10.1111/j.1945-5100.2010.01094.x

Gorai, P., Bhat, B., Sil, M., et al. 2020, ApJ, 895, 86, doi: 10.3847/1538-4357/ab8871

Gorai, P., Das, A., Das, A., et al. 2017a, ApJ, 836, 70, doi: 10.3847/1538-4357/836/1/70

Gorai, P., Das, A., Majumdar, L., et al. 2017b, Molecular Astrophysics, 6, 36, doi: 10.1016/j.molap.2017.01.004

Graedel, T. E., Langer, W. D., & Frerking, M. A. 1982, ApJS, 48, 321, doi: 10.1086/190780

Heyl, J., Sellentin, E., Holdship, J., & Viti, S. 2022, MNRAS, 517, 38, doi: 10.1093/mnras/stac2652

Hincelin, U., Chang, Q., & Herbst, E. 2015, A&A, 574, A24, doi: 10.1051/0004-6361/201424807

Jackson, P., Robinson, K., Puxty, G., & Attalla, M. 2009, Energy Procedia, 1, 985

Jones, P. A., Cunningham, M. R., Godfrey, P. D., & Cragg, D. M. 2007, MNRAS, 374, 579, doi: 10.1111/j.1365-2966.2006.11175.x

Jørgensen, J. K., van der Wiel, M. H. D., Coutens, A., et al. 2016, A&A, 595, A117, doi: 10.1051/0004-6361/201628648

Kameneva, S. V., Tyurin, D. A., & Feldman, V. I. 2017, PCCP (Incorporating Faraday Transactions), 19, 24348, doi: 10.1039/C7CP03518G

Krasnokutski, S. A. 2021, Low Temperature Physics, 47, 199, doi: 10.1063/10.0003519

Krueger, P. J., & Mettee, H. D. 1965, Canadian Journal of Chemistry, 43, 2970

Kuan, Y.-J., Charnley, S. B., Huang, H.-C., Tseng, W.-L., & Kisiel, Z. 2003, ApJ, 593, 848, doi: 10.1086/375637

Kvenvolden, K. A., Lawless, J. G., & Ponnamperuma, C. 1971, Proceedings of the National Academy of Sciences, 68, 486

Lu, H.-C., Chen, H.-K., Cheng, B.-M., & Ogilvie, J. F. 2008, Spectrochimica Acta Part A: Molecular and Biomolecular Spectroscopy, 71, 1485

McGuire, B. A. 2022, ApJS, 259, 30, doi: 10.3847/1538-4365/ac2a48

Millar, T. J., Walsh, C., Van de Sande, M., & Markwick, A. J. 2024, A&A, 682, A109, doi: 10.1051/0004-6361/202346908

Molinari, S., Brand, J., Cesaroni, R., & Palla, F. 2000, A&A, 355, 617, doi: 10.48550/arXiv.astro-ph/0001231

Molpeceres, G., & Rivilla, V. M. 2022, A&A, 665, A27, doi: 10.1051/0004-6361/202243892

Mondal, S. K., Gorai, P., Sil, M., et al. 2021, The Astrophysical Journal, 922, 194, doi: 10.3847/1538-4357/ac1f31

Nazari, P., Cheung, J. S. Y., Ferrer Asensio, J., et al. 2024, arXiv e-prints, arXiv:2401.04760, doi: 10.48550/arXiv.2401.04760

Novakovskaya, Y. V., & Rodnikova, M. N. 2015, Structural Chemistry, 26, 177

Nuevo, M., Auger, G., Blanot, D., & d'Hendecourt, L. 2008, Origins of Life and Evolution of Biospheres, 38, 37

Oba, Y., Tomaru, T., Kouchi, A., & Watanabe, N. 2019, ApJ, 874, 124, doi: 10.3847/1538-4357/ab0961

Penn, R. E., & Curl, R. F. 1971, The Journal of Chemical Physics, 55, 651

Ramachandran, R., Rahul, K., Meka, J., et al. 2023, Journal of Chemical Sciences, 135, 77, doi: https://doi.org/10.1007/s12039-023-02192-z

Redondo, P., Largo, A., & Barrientos, C. 2015, A&A, 579, A125, doi: 10.1051/0004-6361/201526548

Rivilla, V. M., Jiménez-Serra, I., Martín-Pintado, J., et al. 2021, Proceedings of the National Academy of Sciences, 118, e2101314118

Rocha, W. R. M., Rachid, M. G., Olsthoorn, B., et al. 2022, A&A, 668, A63, doi: 10.1051/0004-6361/202244032

Ruaud, M., Wakelam, V., & Hersant, F. 2016, MNRAS, 459, 3756, doi: 10.1093/mnras/stw887

Sil, M., Gorai, P., Das, A., et al. 2018, ApJ, 853, 139, doi: 10.3847/1538-4357/aa984d

Sil, M., Srivastav, S., Bhat, B., et al. 2021, arXiv e-prints, arXiv:2105.14569. https://arxiv.org/abs/2105.14569

Singh, A., Shivani, Misra, A., & Tandon, P. 2013, Research in Astronomy and Astrophysics, 13, 912, doi: 10.1088/1674-4527/13/8/003

Sivaraman, B., Sekhar, B. R., Jones, N., Hoffmann, S., & Mason, N. 2012, Chemical Physics Letters, 554, 57

Srivastav, S., Sil, M., Gorai, P., et al. 2022, Monthly Notices of the Royal Astronomical Society, 515, 3524, doi: 10.1093/mnras/stac1904

Suzuki, T., Majumdar, L., Ohishi, M., et al. 2018, ApJ, 863, 51, doi: 10.3847/1538-4357/aad087

Taniguchi, K., Sanhueza, P., Olguin, F. A., et al. 2023, The Astrophysical Journal, 950, 57, doi: 10.3847/1538-4357/acca1d

Tinacci, L., Germain, A., Pantaleone, S., et al. 2022, ACS Earth and Space Chemistry, 6, 1514, doi: 10.1021/acsearthspacechem.2c00040

Tomasi, J., Mennucci, B., & Cammi, R. 2005, Chemical Reviews, 105, 2999, doi: 10.1021/cr9904009

Viti, S., Collings, M. P., Dever, J. W., McCoustra, M. R. S., & Williams, D. A. 2004, MNRAS, 354, 1141, doi: 10.1111/j.1365-2966.2004.08273.x

Wakelam, V., Loison, J. C., Hickson, K. M., & Ruaud, M. 2015, MNRAS, 453, L48, doi: 10.1093/mnrasl/slv097

Wakelam, V., Loison, J. C., Mereau, R., & Ruaud, M. 2017, Molecular Astrophysics, 6, 22, doi: 10.1016/j.molap.2017.01.002

Widicus, S. L., Drouin, B. J., Dyl, K. A., & Blake, G. A. 2003, Journal of Molecular Spectroscopy, 217, 278

Wirström, E. S., Bergman, P., Hjalmarson, Å., & Nummelin, A. 2007, A&A, 473, 177

Woon, D. E. 2002, ApJL, 571, L177, doi: 10.1086/341227

Zucconi, A., Walmsley, C. M., & Galli, D. 2001, A&A, 376, 650, doi: 10.1051/0004-6361:20010778

APPENDIX

A. GAS PHASE DESTRUCTION REACTIONS OF ETHANOLAMINE AND RELATED SPECIES

The following reactions are included in our network for destroying gas phase ethanolamine and related species. The format of this reaction follows the standard UMIST 2022 network.

```
:IN:H3+:HNCCO:NH3:HC2O+:::1:1.00e-09:-0.50:0.0:10:41000
:IN:HCO+:HNCCO:HNCO:HC2O+:::1:1.00e-09:-0.50:0.0:10:41000
:IN:He+:HNCCO:He:HC2O+:N::1:1.00e-09:-0.50:0.0:10:41000
:IN:H+:HNCCO:NH:HC2O+:::1:1.00e-09:-0.50:0.0:10:41000
:IN:C+:HNCCO:CN:HC2O+:::1:1.00e-09:-0.50:0.0:10:41000
:IN:H3+:NH2CCO:NH3:HC2O+:H::1:1.00e-09:-0.50:0.0:10:41000
:IN:HCO+:NH2CCO:HNCO:HC2O+:H::1:1.00e-09:-0.50:0.0:10:41000
:IN:He+:NH2CCO:He:HC2O+:NH::1:1.00e-09:-0.50:0.0:10:41000
:IN:H+:NH2CCO:NH2:HC2O+:::1:1.00e-09:-0.50:0.0:10:41000
:IN:C+:NH2CCO:HCN:HC2O+:::1:1.00e-09:-0.50:0.0:10:41000
:IN:H3+:NH2CHCO:NH3:HC2O+:H2::1:1.00e-09:-0.50:0.0:10:41000
:IN:HCO+:NH2CHCO:HNCO:HC2O+:H2::1:1.00e-09:-0.50:0.0:10:41000
:IN:He+:NH2CHCO:He:HC2O+:NH2::1:1.00e-09:-0.50:0.0:10:41000
:IN:H+:NH2CHCO:NH3:HC2O+:::1:1.00e-09:-0.50:0.0:10:41000
:IN:C+:NH2CHCO:H2CN:HC2O+:::1:1.00e-09:-0.50:0.0:10:41000
:IN:H3+:NH2CH2CO:NH4+:CH:H2CO::1:1.00e-09:-0.50:0.0:10:41000
:IN:HCO+:NH2CH2CO:NH3:HCO:HC2O+::1:1.00e-09:-0.50:0.0:10:41000
:IN:He+:NH2CH2CO:NH3:He:HC2O+::1:1.00e-09:-0.50:0.0:10:41000
:IN:H+:NH2CH2CO:NH3:HC2O+:H::1:1.00e-09:-0.50:0.0:10:41000
:IN:C+:NH2CH2CO:NH3:HC2O+:C::1:1.00e-09:-0.50:0.0:10:41000
:IN:H3+:NH2CH2CHO:NH4+:CH2:H2CO::1:1.00e-09:-0.50:0.0:10:41000
:IN:HCO+:NH2CH2CHO:NH3:H2CO:HC2O+::1:1.00e-09:-0.50:0.0:10:41000
:IN:He+:NH2CH2CHO:CH4:He:HNCO::1:1.00e-09:-0.50:0.0:10:41000
:IN:H+:NH2CH2CHO:NH3:HC2O+:H2::1:1.00e-09:-0.50:0.0:10:41000
:IN:C+:NH2CH2CHO:NH3:HC2O+:CH::1:1.00e-09:-0.50:0.0:10:41000
:IN:H3+:NH2C2H3OH:NH4+:CH3:H2CO::1:1.00e-09:-0.50:0.0:10:41000
:IN:HCO+:NH2C2H3OH:NH2:CH3OH:HC2O+::1:1.00e-09:-0.50:0.0:10:41000
:IN:He+:NH2C2H3OH:HCN:He:CH3OH2+::1:1.00e-09:-0.50:0.0:10:41000
:IN:H+:NH2C2H3OH:NH4+:H2CO:CH::1:1.00e-09:-0.50:0.0:10:41000
:IN:C+:NH2C2H3OH:NH4+:H2CO:C2::1:1.00e-09:-0.50:0.0:10:41000
:IN:H3+:NH2CH2CH2O:NH4+:CH3:H2CO::1:1.00e-09:-0.50:0.0:10:41000
:IN:HCO+:NH2CH2CH2O:NH2+:CH3CHO:HCO::1:1.00e-09:-0.50:0.0:10:41000
:IN:He+:NH2CH2CH2O:NH2+:He:CH3CHO::1:1.00e-09:-0.50:0.0:10:41000
:IN:H+:NH2CH2CH2O:NH4+:H2CO:CH::1:1.00e-09:-0.50:0.0:10:41000
:IN:C+:NH2CH2CH2O:NH4+:H2CO:C2::1:1.00e-09:-0.50:0.0:10:41000
:IN:H3+:NH2CH2CH2OH:NH3:CH5+:H2CO::1:1.00e-09:-0.50:0.0:10:41000
:IN:HCO+:NH2CH2CH2OH:OCN:CH3:CH3OH2+::1:1.00e-09:-0.50:0.0:10:41000
:IN:He+:NH2CH2CH2OH:H2CN:He:CH3OH2+::1:1.00e-09:-0.50:0.0:10:41000
:IN:H+:NH2CH2CH2OH:NH4+:H2CO:CH2::1:1.00e-09:-0.50:0.0:10:41000
:IN:C+:NH2CH2CH2OH:NH4+:H2CO:C2H::1:1.00e-09:-0.50:0.0:10:41000
:IN:H3+:NH2CH:NH4+:CH2:::1:1.00e-09:-0.50:0.0:10:41000:E:C::
:IN:HCO+:NH2CH:NH4+:C2O:::1:1.00e-09:-0.50:0.0:10:41000:E:C::
:IN:He+:NH2CH:NH3:C+:He::1:1.00e-09:-0.50:0.0:10:41000:E:C::
:IN:H+:NH2CH:NH4+:C:::1:1.00e-09:-0.50:0.0:10:41000:E:C::
```

:IN:C+:NH2CH:NH3:C2+:::1:1.00e-09:-0.50:0.0:10:41000:E:C::
:IN:H3+:NH2CH2:NH4+:CH3:::1:1.00e-09:-0.50:0.0:10:41000:E:C::
:IN:HCO+:NH2CH2:NH4+:C2O:H::1:1.00e-09:-0.50:0.0:10:41000:E:C::
:IN:He+:NH2CH2:NH3:CH+:He::1:1.00e-09:-0.50:0.0:10:41000:E:C::
:IN:H+:NH2CH2:NH4+:CH:::1:1.00e-09:-0.50:0.0:10:41000:E:C::
:IN:C+:NH2CH2:NH3:C2H+:::1:1.00e-09:-0.50:0.0:10:41000:E:C::
:IN:H3+:C3H7NO2:NH4+:CH2CO:CH3OH::1:1.00e-09:-0.50:0.0:10:41000
:IN:H+:C3H7NO2:NH4+:CH3CHO:CO::1:1.00e-09:-0.50:0.0:10:41000
:IN:H3+:C2H4OH:H3O+:C2H5:::1:1.00e-09:-0.50:0.0:10:41000:E:C::
:IN:H+:C2H4OH:H3O+:C2H3:::1:1.00e-09:-0.50:0.0:10:41000:E:C::
:IN:HCO+:C2H4OH:H3O+:C2H3:CO::1:1.00e-09:-0.50:0.0:10:41000:E:C::
:IN:He+:C2H4OH:He:C2H4:OH+::1:1.00e-09:-0.50:0.0:10:41000:E:C::
:IN:C+:C2H4OH:HCO+:C2H4:::1:1.00e-09:-0.50:0.0:10:41000:E:C::
:CR:HNCCO:CRPHOT:NH:C2O:::1:1.30e-17:0.00:1500.0:10:41000:M:C
:CR:NH2CCO:CRPHOT:NH2:C2O:::1:1.30e-17:0.00:1500.0:10:41000:M:C
:CR:NH2CHCO:CRPHOT:NH3:C2O:::1:1.30e-17:0.00:1500.0:10:41000:M:C
:CR:NH2CH2CO:CRPHOT:NH2:CH2CO:::1:1.30e-17:0.00:1500.0:10:41000:M:C
:CR:NH2CH2CHO:CRPHOT:NH2:CH2CHO:::1:1.30e-17:0.00:1500.0:10:41000:M:C
:CR:NH2CH2CH2O:CRPHOT:NH2:CH3CHO:::1:1.30e-17:0.00:1500.0:10:41000:M:C
:CR:NH2CH2CH2OH:CRPHOT:NH3:CH3CHO:::1:1.30e-17:0.00:1500.0:10:41000:M:C
:CR:NH2C2H3OH:CRPHOT:NH2:CH3CHO:::1:1.30e-17:0.00:1500.0:10:41000:M:C
:CR:NH2CH:CRPHOT:NH2:CH:::1:1.30e-17:0.00:1500.0:10:41000:M:C
:CR:NH2CH2:CRPHOT:NH2:CH2:::1:1.30e-17:0.00:1500.0:10:41000:M:C
:CR:C3H7NO2:CRPHOT:H2:CH3CHO:HNCO::1:1.30e-17:0.00:1500.0:10:41000:M:C
:CR:C2H4OH:CRPHOT:C2H4:OH:::1:1.30e-17:0.00:1500.0:10:41000:M:C
:PH:HNCCO:PHOTON:NH:C2O:::1:1.00e-10:0.00:2.0:10:41000:M:C
:PH:NH2CCO:PHOTON:NH2:C2O:::1:1.00e-10:0.00:2.0:10:41000:M:C
:PH:NH2CHCO:PHOTON:NH3:C2O:::1:1.00e-10:0.00:2.0:10:41000:M:C
:PH:NH2CH2CO:PHOTON:NH2:CH2CO:::1:1.00e-10:0.00:2.0:10:41000:M:C
:PH:NH2CH2CHO:PHOTON:NH2:CH2CHO:::1:1.00e-10:0.00:2.0:10:41000:M:C
:PH:NH2CH2CH2O:PHOTON:NH2:CH3CHO:::1:1.00e-10:0.00:2.0:10:41000:M:C
:PH:NH2CH2CH2OH:PHOTON:NH3:CH3CHO:::1:1.00e-10:0.00:2.0:10:41000:M:C
:PH:NH2C2H3OH:PHOTON:NH2:CH3CHO:::1:1.00e-10:0.00:2.0:10:41000:M:C
:PH:NH2CH:PHOTON:NH2:CH:::1:1.00e-10:0.00:2.0:10:41000:M:C
:PH:NH2CH2:PHOTON:NH2:CH2:::1:1.00e-10:0.00:2.0:10:41000:M:C
:PH:C3H7NO2:PHOTON:H2:CH3CHO:HNCO::1:1.00e-10:0.00:2.0:10:41000:M:C
:PH:C2H4OH:PHOTON:C2H4:OH:::1:1.00e-10:0.00:2.0:10:41000:M:C